Acta Chemica Scandinavica A 39 (1985) 671–680

Structural and Magnetic Phase Diagram for the MnAs–CrAs System

HELMER FJELLVÅG and ARNE KJEKSHUS

Kjemisk Institutt, Universitetet i Oslo, Blindern, N-0315 Oslo 3, Norway

The structural and magnetic phase diagram for the MnAs–CrAs system has been studied by X-ray diffraction, differential scanning calorimetry and magnetic susceptibility measurements. Five distinct solid solution phases have been identified, the crystal structure being of the NiAs or MnP type and the magnetic state consisting of para-(P), ferro-(F) or helimagnetic (H_a or H_c) arrangement. The MnP,P⇄NiAs,P ($0.00 \leqq t \leqq 1.00$) and MnP,H_c⇄MnP,P ($0.325 \pm 0.005 \leqq t \leqq 0.88 \pm 0.02$) type transitions are second order (or weakly first order for the latter), all other solid state transitions in the MnAs–CrAs system being first order. A triple point (critical end point) between the MnP,H_a, MnP,H_c and MnP,P type phases is located at 195 ± 1 K and $t = 0.325 \pm 0.005$. The MnP,H_c to MnP,P type transition converts from second (or weakly first) to first order at 293 ± 2 K, $t = 0.88 \pm 0.02$ (pseudo tricritical point).

Several recent studies [1–11] have been concerned with the structural and magnetic properties of the ternary (pseudo binary) MnAs–CrAs system. The phase diagram for the $Mn_{1-t}Cr_tAs$ solid solution phase contains, as a function of temperature and composition, several regions characterized by different structural and/or magnetic states. The present authors have recently reported [11] on the properties of $Mn_{1-t}Cr_tAs$ in the composition range $0.20 \leqq t \leqq 0.40$, where there occurs a first order transition, accompanied by large changes in unit cell dimensions, between two helimagnetically ordered states. However, the details of the temperature and composition dependence of the phase boundaries were left open for a small composition range around $t = 0.35$. In this communication we attempt to complete the phase diagram for this composition range and to provide a more complete covering of the entire t interval ($0.00 \leqq t \leqq 1.00$). Certain discrepancies with findings reported in Refs. 5–10 can probably be attributed to effects of sample preparation, and these aspects will be discussed in a separate paper.[12]

EXPERIMENTAL

The samples of $Mn_{1-t}Cr_tAs$ were synthesized from MnAs and CrAs in evacuated, sealed silica tubes according to the procedure described in Ref. 11. Samples were prepared in steps of $\Delta t = 0.01$ for $0.00 \leqq t \leqq 0.10$, $\Delta t = 0.05$ for $0.10 \leqq t \leqq 0.30$, $\Delta t = 0.005$ for $0.30 \leqq t \leqq 0.40$, $\Delta t = 0.05$ for $0.40 < \Delta t \leqq 0.80$, and $\Delta t = 0.02$ for $0.80 \leqq t \leqq 1.00$. The homogeneity and structural state of the samples were evaluated from room temperature powder X-ray diffraction photographs (Guinier technique, Cu$K\alpha_1$ radiation, Si as internal standard). High and low temperature powder X-ray diffraction data were collected between 90 and 1000 K

0302-4377/85 $2.50

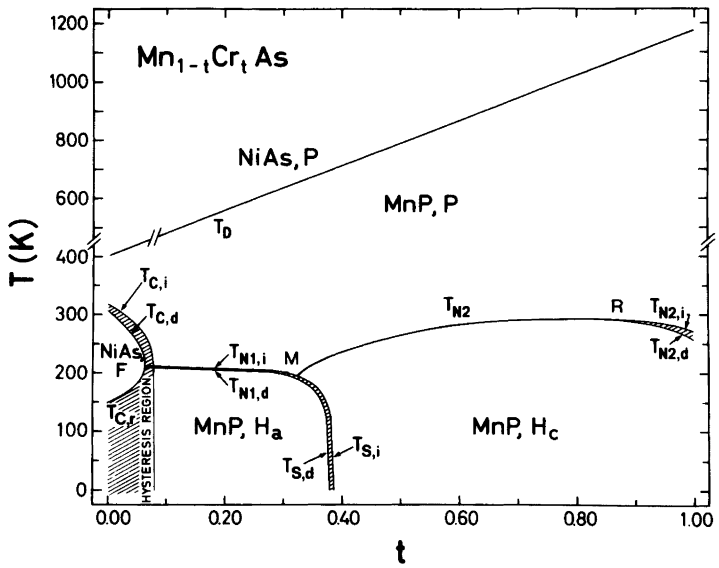

Fig. 1. Structural and magnetic phase diagram for $Mn_{1-t}Cr_tAs$. Legends to notations are given in Table 1.

with an Enraf-Nonius camera based on the Guinier Simon technique, and unit cell dimensions were deduced through least squares refinements.

Differential scanning calorimetry (DSC) measurements were performed between 100 and 900 K using a Mettler TA 3000 system. Magnetic susceptibility data were collected on a conventional Faraday balance (maximum field ~8 kOe; 10–20 mg samples) between 90 and 1000 K.

RESULTS AND DISCUSSION

The structural and magnetic (t,T) phase diagram for $Mn_{1-t}Cr_tAs$ surveyed in Fig. 1 contains five distinct solid solution phases. The crystal structures of these phases are of either the

Table 1. Notations used to specify different phase transitions for $Mn_{1-t}Cr_tAs$. Structural state is indicated by type designation, magnetic state by P=para, F=ferro and H=helical. Subscript *a* or *c* denotes propagation direction of magnetic spirals.

Transition notation	Transition specification	Temperature named
T_D	MnP,P⇄NiAs,P	Distortion
$T_{C,i}$	NiAs,F→MnP,P	Curie (increasing)
$T_{C,d}$	NiAs,F←MnP,P	Curie (decreasing)
$T_{C,r}$	MnP,H_a→NiAs,F	Curie (re-entrant)
$T_{N1,i}$	MnP,H_a→MnP,P	Néel (increasing)
$T_{N1,d}$	MnP,H_a←MnP,P	Néel (decreasing)
T_{N2}	MnP,H_c⇌MnP,P	Néel
$T_{N2,i}$	MnP,H_c→MnP,P	Néel (increasing)
$T_{N2,d}$	MnP,H_c←MnP,P	Néel (decreasing)
$T_{S,i}$	MnP,H_a→MnP,H_c	Spiral (increasing)
$T_{S,d}$	MnP,H_a←MnP,H_c	Spiral (decreasing)

NiAs or MnP type (both referred to in terms of space group *Pnma*, the two kinds of metal atoms being distributed at random over the metal sub-lattice), and the magnetic state consists of either a para-(P), ferro-(F) or helimagnetic (H) arrangement. (Sub-classification of the helimagnetic structures is made according to the propagation direction of the spirals, as indicated by the subscripts *a* and *c*.) A listing of the notations used to denote the different phase transitions shown on Fig. 1 is given in Table 1. The various transition lines and singularity points on Fig. 1 are considered separately below.

(i) *The MnP,P⇄NiAs,P type transition* involves continuous displacive shifts of the metal (T=Mn,Cr) and non-metal (X=As) atoms.[13–15] Parallel with the crystallographic MnP← NiAs type deformation there occurs a reduction of the paramagnetic moment which *inter alia* is manifested by anomalous magnetic susceptibility curves.[3,5,7,9–11]

The values for T_D as a function of the compositional parameter t (Fig. 2) are evaluated from high temperature X-ray diffraction and magnetic susceptibility data. On cooling through T_D some of the reflections characteristic of the NiAs type atomic arrangement (space group $P6_3/mmc$) split up due to the orthorhombic MnP type distortion, and this splitting as well as the appearance of additional reflections can easily be detected. T_D is most conveniently and accurately established by visual inspection of the photographs. However, the temperature dependence of the unit cell dimensions for $Mn_{0.45}Cr_{0.55}As$ and $Mn_{0.35}Cr_{0.65}As$ shown in Fig. 3 can serve as representative examples of the thermal expansion characteristics obtained around the MnP⇄NiAs type phase transition.

The compositional variation of T_D established in Fig. 2 agrees quite well with the findings of Kazama and Watanabe.[3] The present T_D *versus* t relationship is, however, closer to linearity than that reported in Ref. 3. (Kazama and Watanabe have probably confused °C with K in the T_D value for CrAs.)

(ii) *The NiAs,F→MnP,P, NiAs,F←MnP,P and MnP,H_a→NiAs,F type transitions* will be considered in a separate paper[16] together with the findings for the corresponding transitions in other transition metal substituted MnAs phases, and only a few brief comments are given here for the sake of completeness. The first order NiAs,F to MnP,P type transition ($0.00 \leqq t \leqq 0.08$) exhibits hysteresis ($\Delta T > 10$ K). The maximum compositional existence region for the NiAs,F type phase is $0.00 \leqq t \leqq 0.05 \pm 0.01$ (at ~220 K) whereas the hysteresis region extends to $t = 0.08 \pm 0.01$. The unit cell volume increases from the MnP,P to the NiAs,F type phase, an effect which mostly originates from magnetostriction. The pressure induced MnP,H_a type state for $0.00 \leqq t \leqq 0.05 \pm 0.01$ transforms on heating at atmospheric pressure (irreversibly) to the NiAs,F type state at $T_{C,r}$.

(iii) *The MnP,H_a→MnP,P and MnP,H_a←MnP,P type transitions* occur in the composition range $0.05 < t \leqq 0.325 \pm 0.005$. The variation of the Néel temperature over this

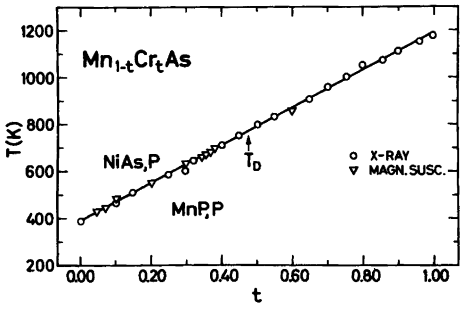

Fig. 2. Variation of T_D with t for $Mn_{1-t}Cr_tAs$ as obtained by high temperature X-ray diffraction and magnetic susceptibility data. Legends to symbols are given on the illustration.

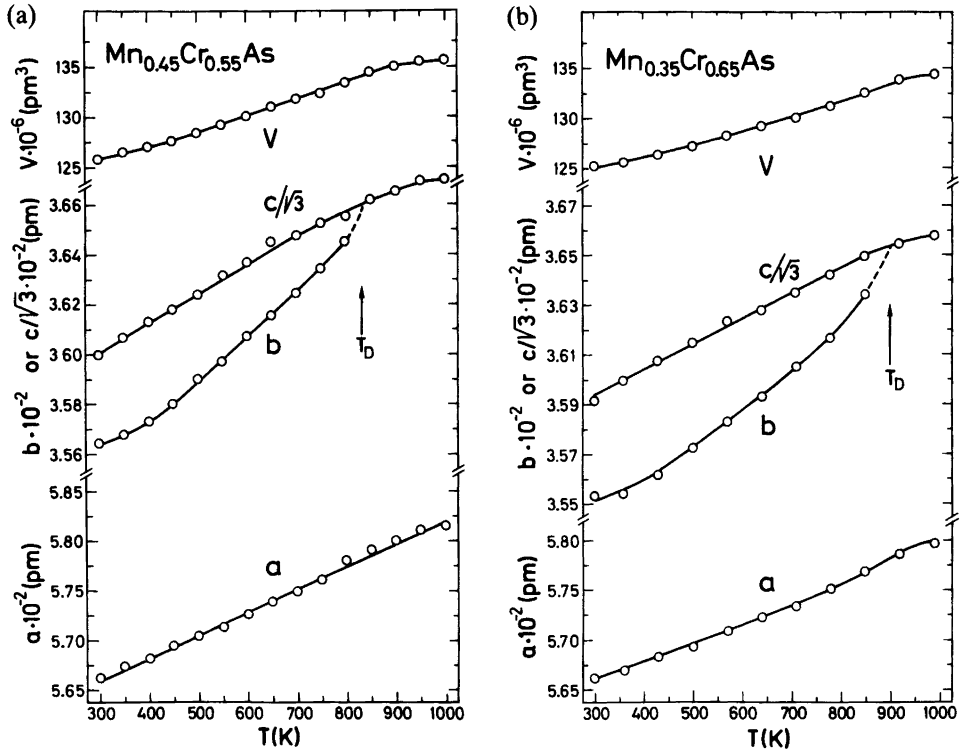

Fig. 3. Unit cell dimensions *versus* temperature for (a) $Mn_{0.45}Cr_{0.55}As$ and (b) $Mn_{0.35}Cr_{0.65}As$ between 300 and 1000 K. *Calculated* error limits do not exceed size of symbols.

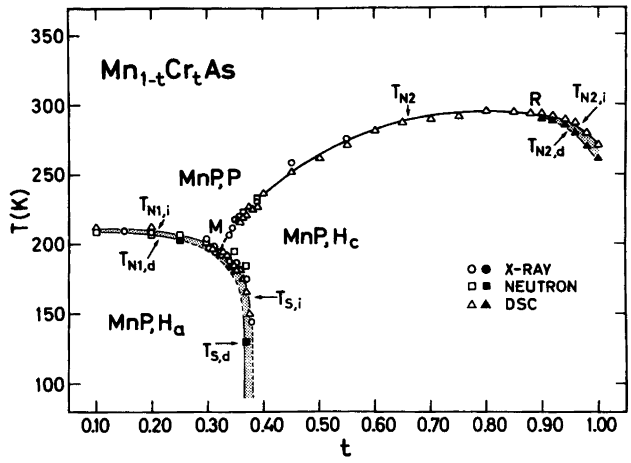

Fig. 4. Magnetic section of $Mn_{1-t}Cr_tAs$ phase diagram for $0.10 \leqq t \leqq 1.00$. Legends to symbols are given on the illlustration; for notations see Table 1. Some data taken from Refs. 4,11 are included. Open and filled symbols refer to data obtained under increasing and decreasing temperature conditions respectively.

appreciable t interval is rather small ($212\pm3 \geqq T_{N1,i} \geqq 195\pm1$ K) and the hysteresis on increasing and decreasing temperature is only slight (say $\Delta T < 4$ K). The first order character of the MnP,H_a to MnP,P type transition, as well as the magnetic states above and below $T_{N1,d}$,$T_{N1,i}$, have been verified by neutron diffraction (*cf.* Refs. 4,11). As documented in Ref. 11 the MnP,H_a to MnP,P type transition is also easily detectable by low temperature X-ray diffraction and DSC. The relevant magnetic section of the $Mn_{1-t}Cr_tAs$ phase diagram for $0.10 \leqq t \leqq 0.325$ shown in Fig. 4 gives $T_{N1,d}$,$T_{N1,i}$ as determined by these techniques. The illustration, which also includes data (DSC, X-ray and neutron diffraction) already reported in Refs. 4,11, shows that the results obtained by the different techniques are in good mutual agreement. The first order MnP,H_a to MnP,P type transition is accompanied by some 2 % discontinuous change in unit cell volume, but only by minor variations in the positional parameters.

The transition in question was first considered in Refs. 2,3 although these authors did not identify the magnetic structure in the co-operative state. The identity of the MnP,H_a type phase was established in Ref. 4, but the first order character of the transition was still overlooked. However, the latter feature is unequivocally documented in Ref. 11, and further evidence is provided by the samples with $0.10 \leqq t \leqq 0.325$ examined in this study. The compositional variation of $T_{N1,d}$, $T_{N1,i}$ shown in Fig. 4 is in excellent agreement with the data reported in Refs. 2,3 for the same composition range.

(iv) *The MnP,H_c ⇄ MnP,P type transition* (*viz.* weakly first or second order conversion between H_c and P magnetic states) takes place in the composition range $0.325\pm0.005 \leqq t \leqq 0.88\pm0.02$. T_{N2} increases with increasing t from 195 ± 1 K for $t=0.325$ through a broad maximum at 295 ± 1 K for $t \approx 0.85$ and obtains a value of 293 ± 2 K at $t=0.88\pm0.02$. As seen from the T_{N2} *versus* t relationship shown in Fig. 4, there is good mutual agreement between the experimental points obtained by the different techniques (DSC and X-ray diffraction).

The MnP,H_c ⇄ MnP,P type transition is manifested as a local minimum in the thermal expansion characteristics of the b axis (which is attributed to magnetostrictive effects below T_{N2}). The unit cell dimensions *versus* temperature relationships ($90 < T < 300$ K) for $t=0.330$, 0.335, 0.340, 0.350, 0.365, 0.45 and 0.55, shown in Fig. 5, may serve as examples of the development in the thermal expansion characteristics as a function of t. For the samples with composition $t=0.330$ and 0.335 (Fig. 5a) the anomaly in the b axis could not be resolved by the low temperature Guinier Simon X-ray diffraction technique (nor by DSC) due to the virtual coincidence between T_{N2} and $T_{S,d}$,$T_{S,i}$. Short and long range order effects originating from a non-uniform distribution of the Mn and Cr atoms over the metal sub-lattice may also contribute to the failure to detect T_{N2} in these samples.

The T_{N2} *versus* t relationship in Fig. 4 resembles closely the corresponding curves in Refs. 2,3, although the latter curves do not bring out the broad maximum described above. There is full consensus (Refs. 2–4,11 and present) about the magnetic states below and above T_{N2} for $\sim 0.50 < t \leqq 1.00$. The main parameter changes associated with the large existence range of the MnP,H_c type phase concern the size of the propagation vector for the spirals, whereas the crystallographic and the other helimagnetic parameters vary remarkably little.

(v) *The MnP,H_a → MnP,H_c and MnP,H_a ← MnP,H_c type transitions* are observed in the comparatively narrow composition interval $0.325\pm0.005 \leqq t \leqq 0.385\pm0.005$. These transitions are connected by hystereses which increase in width from ΔT ($=T_{S,i}-T_{S,d}$) ≈ 10 K for $t=0.325$ to $\Delta T > 50$ K for $t=0.380$. $T_{S,i}$ decreases rapidly from 195 ± 1 K at $t=0.325\pm0.005$ to 0 K at $t=0.385\pm0.005$ ($T_{S,d}$ behaves similarly). The MnP,H_a → MnP,H_c and MnP,H_a ← MnP,H_c type transitions are clearly manifested in DSC, X-ray (*cf.* Figs. 5b-d and Ref. 11) and neutron (*cf.* Ref. 11) diffraction measurements, and the transition temperatures

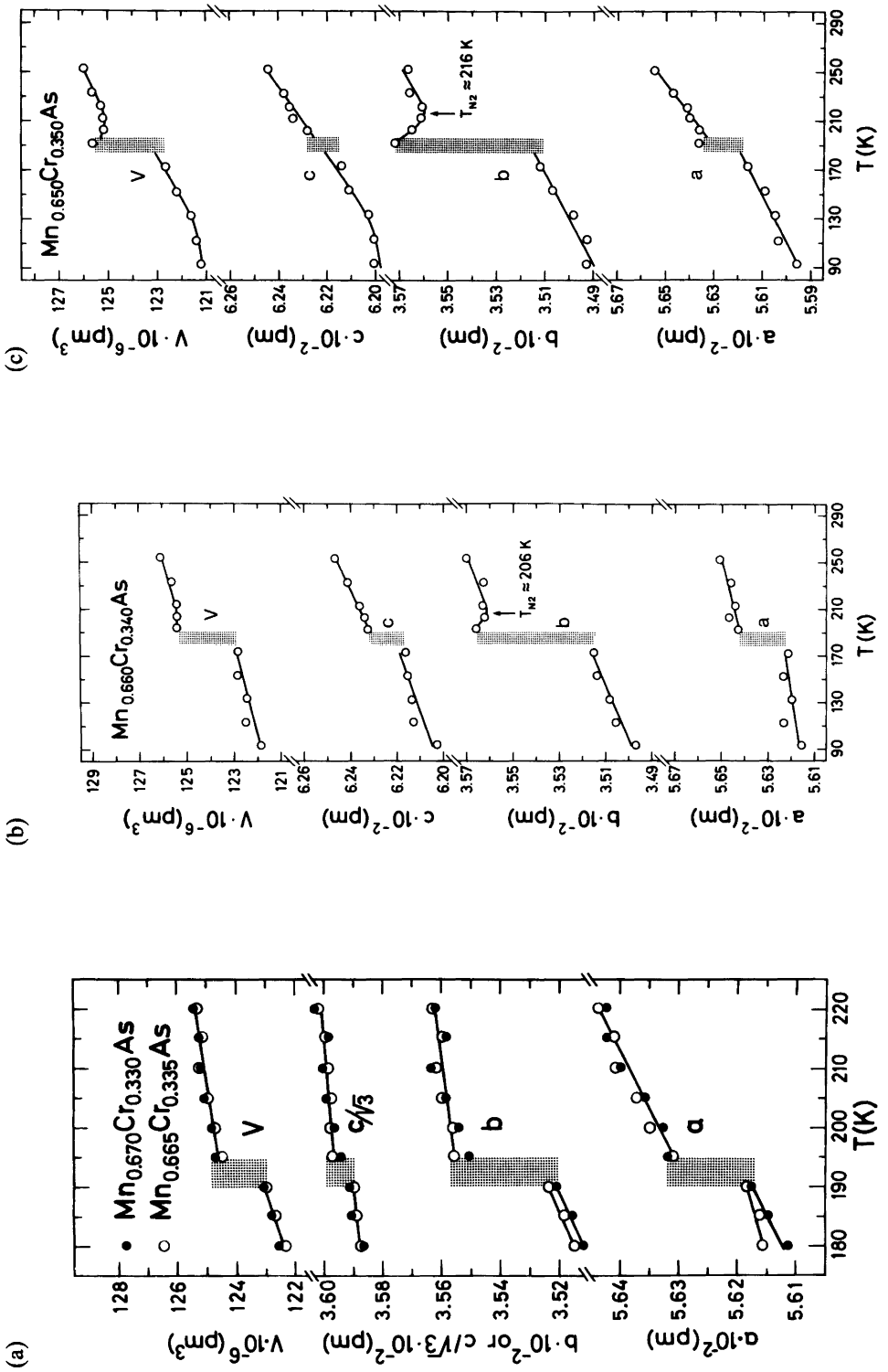
(a)
(b)
(c)
Mn0.670Cr0.330As
Mn0.665Cr0.335As
Mn0.660Cr0.340As
Mn0.650Cr0.350As
T(K)
a·10²(pm)
b·10²or c/√3·10²(pm)
V·10⁶(pm³)
TN2≈216 K
TN2≈206 K

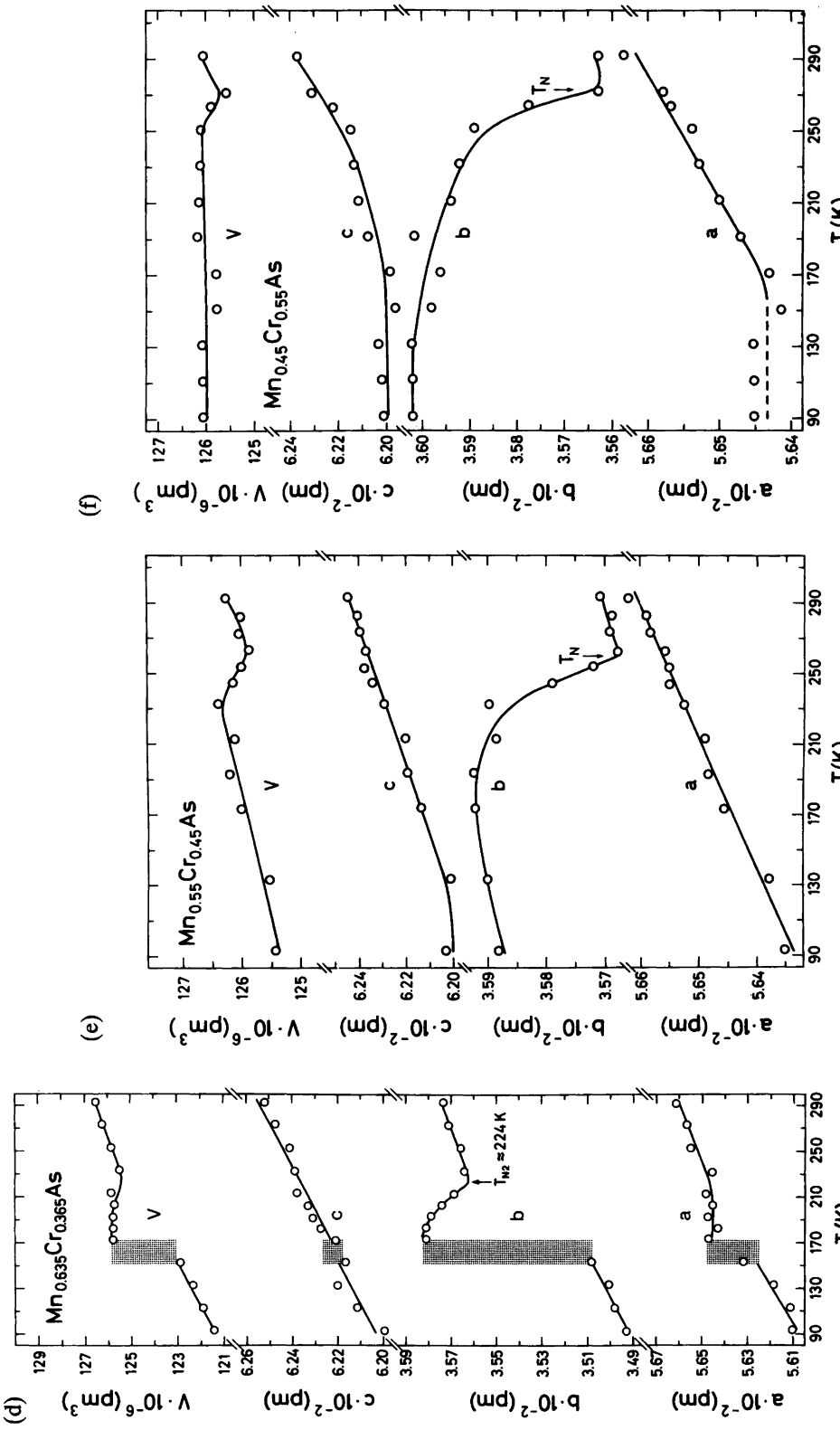

Fig. 5. Temperature dependence of unit cell dimensions for $Mn_{1-t}Cr_tAs$ with (a) t=0.330 and 0.335, (b) t=0.340, (c) t=0.350, (d) t=0.365, (e) t=0.45 and (f) t=0.55. *Calculated* error limits do not exceed the size of symbols. Shaded regions represent the hystereses between MnP,H_a and MnP,H_c type states. Legends to notations are given in Table 1.

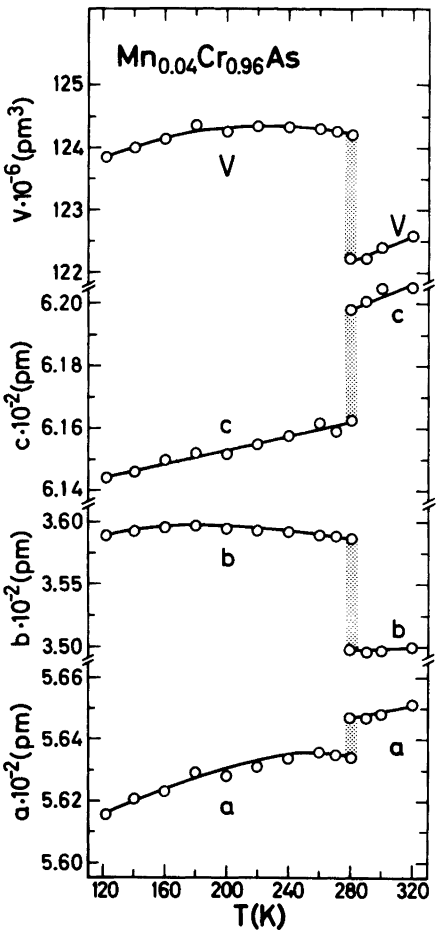

Fig. 6. Unit cell dimensions *versus* temperature for $Mn_{0.04}Cr_{0.96}As$ between 120 and 320 K. *Calculated* error limits do not exceed the size of symbols.

obtained by the different methods match very well (Fig. 4).

The MnP,H_a→MnP,H_c and MnP,H_a←MnP,H_c type transitions are accompanied by distinct changes in the unit cell dimensions (Figs. 5b-d), whereas the positional parameters are only slightly affected.[11] [The average interatomic T–As distance is changed by ~1 % at the transition, whereas the main alteration in the interatomic T–T distances concerns the third shortest separation (identical with *b*, *cf.* Fig. 5).] There appears to be no significant difference in magnetic moment between the H_a and H_c states. The driving force of these transitions is not yet disclosed, but a fair change in free energy appears to be involved.[11]

The MnP,H_a→MnP,H_c and MnP,H_a←MnP,H_c type transitions were not considered in Refs. 2,3. Instead these papers attribute a ferromagnetic low temperature state to the range $\sim 0.35 < t < \sim 0.45$. This distinction may originate from differences in sample preparation and this aspect will be the subject of Ref. 12.

(vi) *The triple point between the MnP,H_a, MnP,H_c and MnP,P type phases* is denoted M in Figs. 1,4. The phase boundaries $T_{N1,d}$ and $T_{N1,i}$ shift notation to $T_{S,d}$ and $T_{S,i}$,

respectively, at M, but the two sets of curves pass continuously into each other. The second order phase boundary T_{N2} meets $T_{N1,i}$–$T_{S,i}$ under an angle at M.

(vii) *The MnP,H_c→MnP,P and MnP,H_c←MnP,P type transitions,* which occur in the composition interval $0.88\pm0.02<t\leqq1.00$, are direct continuations of the corresponding second (or weakly first) order conversion described in section (iv). The T_{N2} phase boundary splits into $T_{N2,d}$ and $T_{N2,i}$ at the pseudo tricritical point R (t=0.88±2, T_{N2}=293±2 K; *cf.* Figs. 1,5). The first order character of the MnP,H_c to MnP,P type transition and the magnetic states above and below $T_{N2,d}$,$T_{N2,i}$ have been established for CrAs by neutron diffraction (*cf.* Refs. 17,18). The transition has been followed through the rest of the ternary region (*i.e.* $0.88<t<1.00$) by low temperature X-ray diffraction and DSC, and the results obtained by the two techniques concur quite well (Fig. 4). The thermal expansion characteristics for $Mn_{0.04}Cr_{0.96}As$ (120–320 K; Fig. 6) bring out the crystallographic component of the MnP,H_c to MnP,P type transition, and show that the unit cell volume of the former state exceeds that of the latter ($\Delta V=2.0\times10^6$ pm^3 for $Mn_{0.04}Cr_{0.96}As$ at $T_{N2,i}$).

$T_{N2,d}$=262±2 K and $T_{N2,i}$=272±2 K for CrAs used in Figs. 1,4 are consistent with the values given in Ref. 17, but at variance (to smaller or larger extent) with those in Refs. 2,3,18–20. The location of the point R is very nearly the same in Refs. 2,3 as in Figs. 1,4. The substitution of small and moderate amounts of MnAs into CrAs produces a negative chemical pressure system (*cf., e.g.,* Refs. 16,21) and the first order behaviour is believed to originate mostly from magnetostriction. (Comparison of Figs. 5f and 6 reveals that the large anomalous thermal expansion of b for $Mn_{0.45}Cr_{0.55}As$ just below T_{N2} is retained also for $Mn_{0.04}Cr_{0.96}As$, although the transition in the latter is discontinuous.) These aspects are currently examined by a variety of methods, and the findings will be reported in a forthcoming paper.[22]

REFERENCES

1. Ido, H. *J. Phys. Soc. Jpn. 27* (1969) 318.
2. Watanabe, H., Kazama, N., Yamaguchi, Y. and Ohashi, M. *J. Appl. Phys. 40* (1969) 1128.
3. Kazama, N. and Watanabe, H. *J. Phys. Soc. Jpn. 30* (1971) 1319.
4. Selte, K., Kjekshus, A., Peterzéns, P.G. and Andresen, A.F. *Acta Chem. Scand. A 32* (1978) 653.
5. Wöhl, R., Krokoszinski, H.J. and Bärner, K. *J. Magn. Magn. Mat. 13* (1979) 119.
6. Wöhl, R., Berg, H. and Bärner, K. *Phys. Stat. Sol. A 57* (1980) 179.
7. Wöhl, R. and Bärner, K. *J. Magn. Magn. Mat. 21* (1980) 80.
8. Krokoszinski, H.J. and Bärner, K. *J. Magn. Magn. Mat. 21* (1980) 221.
9. Tebbe, J. and Bärner, K. *J. Magn. Magn. Mat. 37* (1983) 283.
10. Bärner, K., Santandrea, C., Neitzel, U. and Gmelin, E. *Phys. Stat. Sol. A 123* (1984) 541.
11. Fjellvåg, H. and Kjekshus, A. *Acta Chem. Scand. A 38* (1984) 1.
12. Andresen, A.F., Bärner, K., Fjellvåg, H., Heinemann, K., Kjekshus, A. and Sondermann, U. *J. Magn. Magn. Mat. In press.*
13. Selte, K. and Kjekshus, A. *Acta Chem. Scand. 27* (1973) 3195.
14. Franzen, H.F., Haas, C. and Jellinek, F. *Phys. Rev. B 10* (1974) 1248.
15. Endresen, K., Furuseth, S., Selte, K., Kjekshus, A., Rakke, T. and Andresen, A.F. *Acta Chem. Scand. A 31* (1977) 249.
16. Zięba, A., Zach, R., Fjellvåg, H. and Kjekshus, A. *J. Phys. Chem. Solids. To be published.*
17. Selte, K., Kjekshus, A., Jamison, W.E., Andresen, A.F. and Engebretsen, J.E. *Acta Chem. Scand. 25* (1971) 1703.

18. Kallel, A., Boller, H. and Bertaut, E.F. *J. Phys. Chem. Solids 35* (1974) 1139.
19. Boller, H. and Kallel, A. *Solid State Commun. 9* (1971) 1699.
20. Blachnik, R., Kudermann, G., Grønvold, F., Alles, A., Falk, B. and Westrum, E.F. *J. Chem. Thermodyn. 10* (1978) 507.
21. Zięba, A., Fjellvåg, H. and Kjekshus, A. *J. Phys. Chem. Solids 46* (1985) 275.
22. Fjellvåg, H., Kjekshus, A. and Zięba, A. *J. Magn. Magn. Mat. To be published.*

Received May 6, 1985.